Laith Jaafer Habeeb, Riyadh S. Al-Turaihi / International Journal of Engineering Research and Applications (IJERA) ISSN: 2248-9622 www.ijera.com
Vol. 3, Issue 4, Jul-Aug 2013, pp.2036-2048

Experimental Study and CFD Simulation of Two-Phase Flow Around Triangular Obstacle in Enlarging Channel

Laith Jaafer Habeeb*, Riyadh S. Al-Turaihi**
*(Mechanical Engineering Dept., University of Technology, Baghdad – Iraq
** (College of Engineering/ Dept. of Mech. Eng., Babylon University, Baghdad – Iraq

ABSTRACT

Visualization experiments and 2D numerical simulations have been performed to study two-phase flow phenomena around a triangular-section cylinder in a rectangular channel enlarged from assembly circular tube of the two phases. Experiments are carried out in the channel with air-water flow with different air and water flow rates. These experiments are aimed to visualize the two phase flow phenomena as well as to study the effect of pressure difference through the channel with the obstacle. All sets of the experimental data in this study are obtained by using a pressure transducer and visualized by a video camera for different water discharges (20, 25, 35 and 45 l/min) and different air discharges (10, 20, 30 and 40 l/min). The ability of the moment density approach to represent bubble population size distribution within a multidimensional CFD code based on the two-fluid model is studied. The results showed that the when air discharge increases, high turbulence is appear which generate more bubbles and waves. Also, in a water slug, bubbles move slower than the liquid.

Keywords **-** smooth enlargement, steady and unsteady turbulent flow, triangle-section cylinder, two-phase flow

I. INTRODUCTION

The understanding of turbulent two-phase bubbly flows is important due to the widespread occurrence of this phenomenon in natural and engineering systems [1]. Many flow regimes in Nuclear Reactor Safety Research are characterized by multiphase flows, with one phase being a liquid and the other phase consisting of gas or vapor of the liquid phase. In the regimes of bubbly and slug flows, a spectrum of different bubble sizes is observed. While dispersed bubbly flows with low gas volume fraction are mostly mono-dispersed, an increase in the gas volume fraction leads to a broader bubble size distribution due to breakup and coalescence of bubbles. The interfacial area is crucially important for the transfer of mass, momentum or heat between the continuous and the dispersed phase; thus, the interfacial area cannot be simply modeled under the assumptions of just the void fraction and a mean diameter. Moreover, the forces acting on the bubbles may depend on their individual size. This is the case not just for drag, but also for non-drag forces [2]. Stratified two-phase flow regimes can occur in the main cooling lines of Pressurized Water Reactors, Chemical plants and Oil pipelines. A relevant problem occurring is the development of wavy stratified flows which can lead to slug generation. In the last decade, the stratified flows are increasingly modeled with computational fluid dynamics (CFD) codes. In CFD, closure models are required that must be validated. The recent improvements of the multiphase flow modeling in the ANSYS code make it now possible to simulate these mechanisms in detail [3].

Van et al. [4] were demonstrated the advantages of discretizing on a staggered grid for the computation of solutions to hyperbolic systems of conservation laws arising from instationary flow of an inviscid fluid with an arbitrary equation of state. Results for a highly nonlinear, nonconvex equation of state obtained with the staggered discretization were compared with those obtained with the Osher scheme for two different Riemann problems. The staggered approach was shown to be superior in simplicity and efficiency, without loss of accuracy. The method has been applied to simulate unsteady sheet cavitation on a NACA0012 hydrofoil. Results showed good agreement with those obtained with a cavity interface tracking method. Eckhard et al. 2009 developed a population balance model in close cooperation between ANSYS-CFX and Forschungszentrum Dresden-Rossendorf and implemented into the CFD-Code CFX. They presented a brief description of the model principles. The capabilities of this model were discussed via the example of a bubbly flow around a half-moon shaped obstacle arranged in a 200 mm pipe. In applying the approach, a deeper understanding of the flow structures is possible and the model allows effects of polydispersion to be investigated. For the complex flow around the obstacle, the general structure of the flow was well reproduced in the simulations. This test case demonstrated the complicated interplay between size dependent bubble migration and the effects of bubble coalescence and breakup on real flows. The closure models that characterize the bubble forces responsible for the simulation of bubble migration showed agreement with the experimental observations. However, clear deviations occur for

bubble coalescence and fragmentation. Mostafa et al. [5] simulated the time dependent characteristics performance of cavitating flow around CAV-2003 hydrofoil using pressure-based finite volume method. A bubble dynamics cavitation model was used to investigate the unsteady behavior of cavitating flow and describe the generation and evaporation of vapor phase. For choosing the turbulence model and mesh size a non cavitating study was conducted. The cavitating study presents an unsteady behavior of the partial cavity attached to the foil at different time steps in the case of cavitation number = 0.8. Moreover, there study was focused on cavitation inception, the shape and general behavior of sheet cavitation, lift and drag forces for different cavitation numbers. Igor et al. [6] performed DNS simulations of two-phase turbulent bubbly channel flow at Re_τ = 180 (Reynolds number based on friction velocity and channel half-width) using a stabilized finite element method (FEM) and a level set approach to track the air/water interfaces. Fully developed turbulent single-phase solutions obtained previously using the same stabilized FEM code were used as the initial flow field, and an appropriate level-set distance field was introduced to represent the air bubbles. Surface tension and gravity forces were used in the simulations to physically represent the behavior of a bubbly air/water two-phase flow having a liquid/gas density ratio of 858.3. The simulation results were averaged to obtain the liquid and gas mean velocity distributions, the local void fractions as well as the local turbulent kinetic energy and dissipation rate of the liquid phase. The liquid phase parameters were compared with the corresponding single-phase turbulent channel flow to determine the bubbles' influence on the turbulence field. Peng et al. [7] carried out the numerical simulation to investigate the gas-liquid two-phase flow in the microchannel for the adhesive dispensing. A 2-D model of microchannel with a diameter for 0.04 mm was established and meshed. The gas-liquid slug flow emerges after iterating over 1 million steps with the gas flow rate for 0.1 m/s, the water flow rate for 0.05 m/s. The wetting property controlled by the contact angle had been discussed to present different liquid materials application. The poor wetting of liquid benefited for conforming droplets shape and avoiding droplets crashing and back haul. While the gas flow rate decreased, the length of liquid droplet and gas bubble increased and decreased, respectively and the total numbers of bubble and droplet decreased in one period. This indicated the fluid parameters have a high relationship with the quantity and volume of droplet. Thomas et al. [8] investigated experimentally and numerically the effect of fluid properties and operating conditions on the generation of gas–liquid Taylor flow in microchannels. Visualization experiments and 2D numerical simulations have been performed to study bubble and slug lengths, liquid film hold-up and bubble velocities. The results showed that the bubble and slug lengths increase as a function of the gas and liquid flow rate ratios. The ratio of the bubble velocity to superficial two-phase velocity is close to unity, which confirms a thin liquid film under the assumption of a stagnant liquid film. Numerical simulations confirm the hypothesis of a stagnant liquid film and provide information on the thickness of the liquid film.

From the previous review it is denoted that the recent researches in the two phase flow with the enlargement and existence of a circular cylinder are very limited. So, our concern in this study is to study the effects of wide range of air/water discharge in the steady and unsteady cases on the flow behavior with the enlargement from the circular tube of the water phases which contains the air phase tube, to the rectangular duct with the existence of a triangle-section cylinder. In order to validate existing and further developed multiphase flow models, high-resolution measurement data is needed in time and also in space. For the experimental investigation of co-current air/water flows, the HAWAC (Horizontal Air/Water Channel) was built. The channel allows in particular the study of air/water slug flow under atmospheric pressure. Parallel to the experiments, CFD calculations were carried out. The behavior of slug generation and propagation was qualitatively reproduced by the simulation.

II. PHYSICAL MODEL AND EXPERIMENTAL APPARATUS

Fig.1 shows a schematic and photograph of the experimental Apparatus and measurements system. The rig is consists of, as shown in Fig. 2:

1-Main water tank of capacity (1 m3).

2-Water pump with specification quantity (0.08 m3/min) and head (8 m).

3-Valves and piping system (1.25 in)

4-Adjustable volume flow rate of range (10-80 l/min) is used to control the liquid (water) volume flow rates that enter test section.

5-Air compressor and it has a specification capacity of (0.5 m3) and maximum pressure of (16 bars).

6-Rotameter was used to control the gas (air) volume flow rates that enter the test section. It has a volume flow rate range of (6-50 l/min).

7-Valves and piping system (0.5 in) and gages.

8-Pressure transducer sensors which are used to record the pressure field with a range of (0-1 bar) and these pressure transducer sensors are located in honeycombs at the entrance and at the end of the test section. The pressure sensors with a distance of (80 cm) between each other are measuring with an accuracy of (0.1%).

9-The obstacle used is made of stainless steel and its dimensions are (3 cm) for each of the triangle sides and (3 cm) for the width, which is coated with a very

thin layer of black paint and its center located at (11.5 cm) from the entrance of the test section.

10-The test section is consisting of rectangular channel and a triangular-section cylinder. The rectangular cross sectional area is (10 cm × 3 cm) and has length of (70 cm) which is used to show the behavior of the two phase flow around the obstacle and to measure the pressure difference and records this behavior. The obstacle is mounted and fixed by screw and nut on a blind panel on the bottom of the rectangular channel. The three large Perspex windows of the channel (two lateral sides with lighting and the top side) allowing optical access through the test section. Two enlargement connecting parts are made of steel and manufactured with smooth slope. The first on is used to connect the test section with the outside water pipe in the entrance side while the second one is used to connect the test section with the outside mixture pipe in the exit side. The inside air pipe, in the entrance side, is holed and contained inside the water pipe by a steel flange.

11-Interface system consists of two parts which are the data logger and the transformer which contains in a plastic box. The data logger has a three connections two of them are connected to the outside of the box (one connected to the sensors and the other connected to the personal computer), the third connection is connected to the transformer, which is work to receive the signals as a voltage from the sensors and transmit it into the transformer and then re-received these signals after converting it to ampere signals in the transformer.

12-The interface system which is connected with a personal computer so that the measured pressure across the test section is displayed directly on the computer screen by using a suitable program.

13-A Sony digital video camera recorder of DCR-SR68E model of capacity 80 GB with lens of Carl Zeiss Vario-Tessar of 60 x optical, 2000 x digital is used to visualize the flow structure. The visualized data are analyzed by using a AVS video convertor software version 8.1. A typical sequence snapshots recorded by the camera using a recording rate of 30 f/s.

The flows of both gas and liquid are regulated respectively by the combination of valves and by-passages before they are measured by gas phase flow meter and liquid phase flow meter. The gas phase and the liquid phase are mixed in the enlargement connection part before they enter the test section. When the two-phase mixture flows out of the test section, the liquid phase and the gas phase are separated in liquid storage tank. Experiments were carried out to show the effect of different operation conditions on pressure difference across the test section and to visualize the flow around the obstacle. These conditions are water discharges and air discharges. The selected experimental values for water discharges are (20, 25, 35 and 45 l/min) and for air discharges are (10, 20, 30 and 40 l/min).

The experimental procedures are:

1- Turn on the water pump at the first value (20 l/min).
2- Turn on the air compressor at the first value (10 l/min).
3- Record the pressure drop through the test section and photograph the motion of the two-phase flow by the digital camera.
4- Repeat the above steps by changing the water discharge.
5- Repeat the above steps by changing the air discharge.

These give sixteen (16) cases for volume fraction (Air/Water ratios).

III. NUMERICAL MODELLING

The computational fluid dynamics (CFD) software have been applied for the numerical simulation for adiabatic gas-liquid flow characteristics through a horizontal channel contain a triangular-section cylinder with smooth expansion from the liquid pipe in steady, unsteady and 2D cases. Air-water couple has been selected as the representative of the gas-liquid two-phase flow. Construction of the numerical domain and the analysis are performed via GAMBIT and FLUENT (ANSYS 13.0) CFD codes, respectively. Two-phase flow variables such as void fraction and flow velocity for liquid (water) and gas (air) at the inlet condition, and the geometrical values of the system (i.e. channel length, width and height, pipes and inlet enlargement connecting part dimensions, and obstacle dimensions) used in the analysis are selected as the same variables as the experimental part. Atmospheric conditions are valid for the experimental facility. Total test rig length in the experiments, thus in the numerical domain, is (100 cm) including (70 cm) for the test section containing obstacle, and (30 cm) for the inlet enlargement part. Water pipe diameter is (3.175 cm) and air pipe diameter is (1.27 cm) as shown in Fig. 3.

The enlargement connecting part length consists of: (0.05 m) circular pipe, (0.15 m) diverge-link to change the shape from circular to rectangular and (0.1 m) rectangular part. Air and water are selected to be working fluids and their fluid properties are in **Table 1**.

Table 1. Property parameters of the gas and liquid in CFD.

Fluid	Density (kg/m^3)	Viscosity (kg/m.s)	Surface Tension
Water	998.2	10.03×10^{-04}	0.072
Air	1.225	1.7894×10^{-05}	---

The model geometry structure was meshed by the preprocessor software of GAMBIT with the Quad/Submap grids. After meshing, the model

contained 14447 grid nodes and 29348 faces for 2D before importing into the processor Fluent for calculation. This refinement grid provided a precise solution to capture the complex flow field around the triangular-section cylinder and mixing region in the enlargement connecting part. The boundary conditions are the velocity inlet to the air and water feeding (Table 2) and the pressure outlet to the model outlet. A full geometry is considered because of the asymmetry behavior of the mixture that appeared in the movies when photographing the experiences as will be shown later. In Fluent, the Mixture model was adopted to simulate the flow. The mixture model is a simplified Eulerian approach for modeling *n*-phase flows **(FLUENT 2006)**. Because the flow rates of the air and water in the channel are high, the turbulent model (*k-ε* Standard Wall Function) has been selected for calculation. The other options in Fluent are selected: SIMPLE (Semi-Implicit Method for Pressure-Linked Equations) scheme for the pressure-velocity coupling, PRESTO (pressure staggering option) scheme for the pressure interpolation, Green-Gauss Cell Based option for gradients, First-order Up-wind Differencing scheme for the momentum equation, the schiller-naumann scheme for the drag coefficient, manninen-et-al for the slip velocity and other selections are described in **Table 3**. The time step (for unsteady case), maximum number of iteration and relaxation factors have been selected with proper values to enable convergence for solution which is about (0.001) for all parameters.

Table 2. Air-water flow cases.

Case number	Air/water discharges (l/min)	Air/water velocities (m/sec)	Case number	Air/water discharge (l/min)	Air/water velocities (m/sec)
1	10/20	1.32/0.50	5	20/20	2.63/0.50
2	10/25	1.32/0.63	6	20/25	2.63/0.63
3	10/35	1.32/0.87	7	20/35	2.63/0.87
4	10/45	1.32/1.12	8	20/45	2.63/1.12
Case number	Air/water discharge (l/min)	Air/water velocities (m/sec)	Case number	Air/water discharge (l/min)	Air/water velocities (m/sec)
9	30/20	3.95/0.50	13	40/20	5.26/0.50
10	30/25	3.95/0.63	14	40/25	5.26/0.63
11	30/35	3.95/0.87	15	40/35	5.26/0.87
12	30/45	3.95/1.12	16	40/45	5.26/1.12

Table 3. The solution methods details and other selections for Fluent.

Spatial Discretization		
Gradient: Green-Gauss Cell Based, Momentum Equation: First-order Up-wind		
Solver type	*k-ε* Model	Solution Methods
Pressure-Based	Cmu=0.09, C1-Epsilon=1.44, C2-Epsilon=1.92	Volume Fraction and Turbulent Kinetic Energy (First-order Up-wind)
Starting Solution Controls (Under-Relaxation Factors)		
Pressure=0.3, Momentum=0.7, Turbulent Kinetic Energy & Turbulent Dissipation Rate=0.8		
Specification Method for turbulence		
Intensity and Hydraulic Diameter (Turbulent Intensity=3% and Hydraulic Diameter=0.0127 m)		

The hydrodynamics of two-phase flow can be described by the equations for the conservation of mass and momentum, together with an additional advection equation to determine the gas-liquid interface. The two-phase flow is assumed to be incompressible since the pressure drop along the axis orientation is small. For the incompressible working fluids, the governing equations of the Mixture Multiphase Model are as following (**FLUENT 2006** & **ANSYS 13)**:

- The continuity equation for the mixture is:

$$\frac{\partial}{\partial t}(\rho_m) + \nabla \cdot (\rho_m \vec{v}_m) = 0 \quad (1)$$

Where $\vec{v}_m$ is the mass-averaged velocity:

$$\vec{v}_m = \frac{\sum_{k=1}^{n} \alpha_k \rho_k \vec{v}_k}{\rho_m} \quad (2)$$

and ρ_m is the mixture density:

$$\rho_m = \sum_{k=1}^{n} \alpha_k \rho_k \quad (3)$$

α_k is the volume fraction of phase *k* .

- The momentum equation for the mixture can be obtained by summing the individual momentum equations for all phases. It can be expressed as:

$$\frac{\partial}{\partial t}(\rho_m \vec{v}_m) + \nabla \cdot (\rho_m \vec{v}_m \vec{v}_m) = -\nabla p + \nabla \cdot [\mu_m (\nabla \vec{v}_m + \nabla \vec{v}_m^T)] + \rho_m \vec{g} + \vec{F} + \nabla \cdot \left(\sum_{k=1}^{n} \alpha_k \rho_k \vec{v}_{dr,k} \vec{v}\right) \quad (4)$$

where *n* is the number of phases, $\vec{F}$ is a body force and μ_m is the viscosity of the mixture:

$$\mu_m = \sum_{k=1}^{n} \alpha_k \mu_k \quad (5)$$

$\vec{v}_{dr,k}$ is the drift velocity for secondary phase *k* :

$$\vec{v}_{dr,k} = \vec{v}_k - \vec{v}_m \quad (6)$$

From the continuity equation for secondary phase *p* , the volume fraction equation for secondary phase *p* can be obtained:

$$\frac{\partial}{\partial t}(\alpha_p \rho_p) + \nabla \cdot (\alpha_p \rho_p \vec{v}_m) = -\nabla \cdot (\alpha_p \rho_p \vec{v}_{dr,p}) + \sum_{q=1}^{n}(\dot{m}_{qp} - \dot{m}_{pq}) \quad (7)$$

The relative velocity (also referred to as the slip velocity) is defined as the velocity of a secondary phase (*p*) relative to the velocity of the primary phase (*q*):

$$\vec{v}_{pq} = \vec{v}_p - \vec{v}_q \quad (8)$$

The mass fraction for any phase (*k*) is defined as:

$$c_k = \frac{\alpha_k \rho_k}{\rho_m} \quad (9)$$

The drift velocity and the relative velocity ($\vec{v}_{qp}$) are connected by the following expression:

$$\vec{v}_{dr,p} = \vec{v}_{pq} - \sum_{k=1}^{n} c_k \vec{v}_{qk} \quad (10)$$

ANSYS FLUENT's mixture model makes use of an algebraic slip formulation. The basic assumption of the algebraic slip mixture model is that to prescribe an algebraic relation for the relative velocity, a local equilibrium between the phases should be reached over a short spatial length scale. The form of the relative velocity is given by:

$$\vec{v}_{pq} = \frac{\tau_p(\rho_p - \rho_m)}{f_{drag}\ \rho_p}\vec{a} \quad (11)$$

where τ_p is the particle relaxation time:

$$\tau_p = \frac{\rho_p d_p^2}{18\mu_q} \quad (12)$$

d is the diameter of the particles (or droplets or bubbles) of secondary phase *p* , $\vec{a}$ is the secondary-phase particle's acceleration. The default drag function f_{drag}:

$$f_{drag} = \begin{cases} 1 + 0.15\,Re^{0.687} & Re \le 1000 \\ 0.0183\,Re & Re > 1000 \end{cases} \quad (13)$$

and the acceleration $\vec{a}$ is of the form:

$$\vec{a} = \vec{g} - (\vec{v}_m \cdot \nabla)\vec{v}_m - \frac{\partial \vec{v}_m}{\partial t} \quad (14)$$

The simplest algebraic slip formulation is the so-called drift flux model, in which the acceleration of the particle is given by gravity and/or a centrifugal force and the particulate relaxation time is modified to take into account the presence of other particles.

In turbulent flows the relative velocity should contain a diffusion term due to the dispersion appearing in the momentum equation for the dispersed phase. ANSYS FLUENT adds this dispersion to the relative velocity:

$$\vec{v}_{pq} = \frac{(\rho_p - \rho_m)d_p^2}{18\mu_q f_{drag}}\vec{a} - \frac{\eta_t}{\sigma_t}\left(\frac{\nabla \alpha_p}{\alpha_p} - \frac{\nabla \alpha_q}{\alpha_q}\right) \quad (15)$$

where σ_t is a Prandtl/Schmidt number set to 0.75 and η_t is the turbulent diffusivity. This diffusivity is calculated from the continuous-dispersed fluctuating velocity correlation, such that:

$$\eta_t = C_\mu \frac{k^2}{\varepsilon}\left(\frac{\gamma_y}{1+\gamma_y}\right)\left(1 + C_\beta \xi_\gamma^2\right)^{-1/2} \quad (16)$$

$$\xi_\gamma = \frac{|\vec{v}_{pq}|}{\sqrt{2/3k}} \quad (17)$$

Where $C_\beta = 1.8 - 1.35\ cos^2\theta$, $cos\theta = \frac{\vec{v}_{pq} \cdot \vec{v}_p}{|\vec{v}_{pq}||\vec{v}_p|}$ and γ_y is the time ratio between the time scale of the energetic turbulent eddies affected by the crossing-trajectories effect and the particle relaxation time. If the slip velocity is not solved, the mixture model is reduced to a homogeneous multiphase model.

In FLUENT application, boundary conditions like "velocity inlet" is taken as the inlet condition for water and air while "interior" and "outflow" are employed as the water-air mixture. Air is injected to the water via an air pipe in the experiments, therefore, the gas flow through the air pipe and the mixture occurred outlet of it are modeled in 3D (Fig. 3). According to the simulation, air with known mass flow rate flows through air pipe and then disperses into the water at the exit of the pipe. At air flow rates (thus volumetric void fraction), phase mass flow rate and void fraction profiles obtained at the air and water pipes outlet are extracted from the experimental calculations in order to be introduced as the inlet condition for the flow analysis regarding the numerical 2D domain. In the present study bubble diameter is equal to (1 cm). Assuming the bubbles are in spherical shape and neglecting the coalescence between them along the channel.

IV. EXPERIMENTAL RESULTS

The experimental results are represented as visualizations of a circular cylinder in gas-liquid flow through channel for different water discharges (20, 25, 35 and 45 l/min) and different air discharge (10, 20, 30 and 40 l/min) as photographs and pressure graphs.

4.1 Effect of Air Discharge

Fig.s (4-a, b, c & d) show photographs for the two phase flow behavior around the triangle body for water discharge (Qw=20 l/min) and air discharges (Qa=10, 20, 30 and 40 l/min) from top to bottom respectively. It shows that the number (amount) of bubble is few and has small size at low air discharge. Photographs (4-a & b) describe the flow behavior and it appears that it is near to slug or plug region. This is due to the low velocity of water at low water discharge. Also when increase the air discharge the size and number of bubbles increases and the bubble cavities develops to cloud cavitations especially at high air discharge. This is due to the high velocity of air at high air discharge which leads to more turbulence in the flow and the flow becomes bubbly as shown in photographs (4-c & d). Fig.s (5-a, b, c & d) show photographs for the two phase flow behavior for water discharge (Qw=25 l/min) and air discharges (Qa=10, 20, 30 and 40 l/min) from top to bottom respectively. It is clear that the flow becomes unstable and unsymmetrical around the triangle body and the number and size of bubble become higher compared with the previous case. It appears that the vortices behind and beside the triangle body becomes more strong compared with the previous case. Fig. 6 represents photographs for the flow behavior around the obstacle for water discharge (Qw=35 l/min) and the same air discharges. While Fig. 7 represents photographs for water discharge (Qa=45 l/min) and the same water discharges. More unsteady behavior is noticed and the flow oscillates between bubble and disperse regions. When air discharge increases with increase water discharge, flow becomes unsteady, vortices developed around the triangle body surface and most bubbles transformed to cloudy flow, then a disperse region and strong vortex shedding is observed.

Also when water discharge increases, high turbulence appears which generate more bubbles and waves. This is due to the important effect of the obstacle existence in rectangular channel which effect on pressure difference across the inlet and the outlet of the channel.

4.2 Effect of Time Evolution of Pressure

Fig. 8 represents the effect of time evolution of pressure obtained by experiments for water discharge Qw=20 l/min and air discharge Qa=10 l/min at inlet and outlet of the rectangular channel. The pressure sensor at the inlet -after honeycombs- and outlet of the test section are record pressures that fluctuating as a function of time due to two-phase effect.

4.3 Effect of Pressure Difference

Fig. 9 represents the mean pressure difference with water discharge for different values of air discharge. While Fig. 10 shows the mean pressure difference with air discharge for different values of water discharge. When air or water discharge increases, the mean pressure difference increases. This is due to the increase of air or water discharge resulting in velocity increases. It is already noticed that the mean pressure difference has a significant influence on the two-phase flow behavior. Therefore, it is expected that the flow instability will also depend upon the pressure difference.

V. NUMERICAL RESULTS

The numerical results are represented as contours and vectors for the same air-water discharges cases in the experimental part (Table 2). As mentioned above, the 2D inlet (line) air or water velocities are calculated from the 3D experimental inlet (surface) area from the air or water discharge.

5.1 Steady State

Fig.s (11-a, b, c, d, e, f, g and h) depict volume fraction (water) contours for selected cases (1, 2, 4, 5, 8, 11, 12 and 13) respectively. The differences between the experimental snapshots and numerical Fig.s are due to two reasons; the first is the differences in the overall flow rates of air and water for the same inlet velocities from the inlet regions (small lines in 2D numerical cases and big square and annulus areas in 3D experimental cases), and the second reason is that the snapshots are taken roughly from the experimental movies for each case and may be for another snapshot from the same case movie, the differences will be less. From Fig. 11 it is appear that a slug to disperse regions flow pattern is achieved. The flow rates of air and water have a large range. The increase in water phase with the decrease of the gas flow rate, the volume fraction of the gas decreased and the volume fraction of the water increased simultaneously. According to the figures, stratified water-air mixture enters the singularity section and begins to decelerate due to the smoothly enlarging cross-section. These figures represent how the volume fraction affected the flow behavior. A uniform dispersed two-phase flow, in which the dispersed phase (air bubbles) moves with their carrier fluid (water), approaches to the obstacle. Due to strong changes of both magnitude and direction of local velocities of the fluid flow (i.e. local fluid velocity gradients) and density difference between the dispersed phase and the fluid, the local phase distribution pattern changes markedly around the obstacle.

Fig.s (12-a, b, c, and d) show selected focused area of velocity vectors colored by volume fraction (water) for other cases (a- case7, b- case10, c- case14 and d- case15) respectively. These figures represent the calculated local velocities in the flow

field around the obstacle with the potential flow region at different air/water velocity ratios. Strong air flows are induced and a strong vortex is created as a result of the entered air and small vortices are also produced. A recirculation zone in the wake, a flow separation at the edge of the obstacle and a wavy motion are noticed. Also, when air velocity increases, separation area is detected after the obstacle.

5.2 Unsteady State

Fig.s (13-a, b, c, and d) represent volume fraction (water) contours development for selected unsteady case3. It show how the volume fraction develops with time. As can be seen, there is an unsteady asymmetrical pattern recirculating zone behind the obstacle when the volume fraction increases or when the two-phase velocity (Reynolds number) increases.

VI. CONCLUSION

The study has focused on phase distributions in low quality dispersed two phase flows around obstacle. It consists of a theoretical part of a more general nature and an experimental part highlighting bubbly flows around a triangle body in horizontal channel. Concluding remarks are summarized below-

1- A novel approach for fluid dispensing with high consistency and accuracy had been proposed based on the fluid dynamics of the gas-liquid two-phase flow.
2- When air discharge increases, high turbulence is appear which generate more bubbles and waves.
3- The pressure sensor at the inlet and outlet of the test section are record pressures that fluctuating as a function of time due to two-phase effect. Also, when air or water discharge increases, the mean pressure difference increases.
4- Due to strong changes of both magnitude and direction of local velocities of the fluid flow and density difference between the dispersed phase and the fluid, the local phase distribution pattern changes markedly around the obstacle.
5- Realistic bubble trajectories, with a number of bubble trajectories entering the wake of a triangular-section cylinder, are only obtained if the effect of liquid velocity fluctuations (or turbulence in the liquid) is simulated and some kind of sliding phenomenon for colliding bubbles is taken into account.
6- The effect of the existence of a triangular-section cylinder is clear in dividing the two-phase flow, generate vortices and finally enhance mixing.
7- In this study, diameter of the bubbles is considered constant and coalescence between the bubbles is neglected. However, bubbles in the actual flow break down and unite as the flow develops along the channel and this gives a varying diameter distribution which causes lift and drag forces to be calculated locally. Therefore, a simulation considering the effects of differing bubble diameter and interfacial forces is suggested for better modeling of the flow investigated.

References

[1] Igor A. Bolotnov, Kenneth E. Jansen, Donald A. Drew, Assad A. Oberai, Richard T. Lahey Jr. and Michael Z. Podowski, "Detached Direct Numerical Simulations of Turbulent Two-Phase Bubbly Channel Flow", *International Journal of Multiphase Flow 37* (2011) 647–659.
[2] Eckhard Krepper, Matthias Beyer, Thomas Frank, Dirk Lucas and Horst-Michael Prasser, CFD Modelling of Polydispersed Bubbly Two-Phase Flow Around an Obstacle, *Nuclear Engineering and Design 239* (2009) 2372–2381.
[3] Thomas HÖHNE, Experiments and Numerical Simulations of Horizontal Two Phase Flow Regimes, *Seventh International Conference on CFD in the Minerals and Process Industries*, CSIRO, Melbourne, Australia, December 2009.
[4] D. R. van der Heul and C. Vuik, P. Wesseling, A Staggered Scheme for Hyperbolic Conservation Laws Applied to Unsteady Sheet Cavitation, *Computing and Visualization in Science, Springer-Verlag, 2:*, 63–68 (1999).
[5] N. Mostafa, M. M. Karim and M. M. A. Sarker, A Study on Numerical Analysis of Unsteady Flow over Two Dimensional Hydrofoils, *Proceedings of MARTEC, The International Conference on Marine Technology*, December 2010, BUET, Dhaka, Bangladesh.
[6] Igor A. Bolotnov, Kenneth E. Jansen, Donald A. Drew, Assad A. Oberai, Richard T. Lahey Jr. and Michael Z. Podowski, Detached Direct Numerical Simulations of Turbulent Two-Phase Bubbly Channel Flow, *International Journal of Multiphase Flow 37* (2011) 647–659.
[7] Peng Peng, Jianhua Zhang and Jinsong Zhang, Simulations for a Novel Fluid Dispensing Technology Based on Gas-liquid Slug Flow, *International Conference on Electronic Packaging Technology & High Density Packaging* IEEE 2011.
[8] Thomas Abadie, Joëlle Aubin, Dominique Legendre, Catherine Xuereb, Hydrodynamics of Gas–Liquid Taylor Flow in Rectangular Microchannels, *Springer-Verlag, Microfluid Nanofluid* (2012) 12:355–369.
[9] Introductory FLUENT Notes, FLUENT v6.3, *Fluent User Services Center*, December 2006.
[10] ANSYS 13.0 Help, *FLUENT Theory Guide*,

Mixture Multiphase Model.

[11] Riyadh S. Al-Turaihi, Experimental Investigation of Two-Phase Flow (Gas – Liquid) Around a Straight Hydrofoil in Rectangular Channel, *Journal of Babylon University*, Iraq, 2012, accepted and submitted for publication.

Nomenclature

c_k	Mass fraction	(-)
d	Diameter of the particles	(m)
$\vec{F}$	Body force	(N)
f_{drag}	Drag function	(-)
$\vec{g}$	Gravity acceleration	(m/s^2)
$\dot{m}$	Mass flow rate	(kg/m^3.s)
n	Number of phases	(-)
Q	Discharge	(l/min)
t	Time	(sec)

Subscripts

a	Air
k,p	Secondary phase
m	Mixture
w	Water

Greek Symbols

α_k	Volume fraction of phase *k*	(-)
$\vec{a}$	Secondary-phase particle's acceleration	(m/s^2)
η_t	Turbulent diffusivity	(N/m^2.s)
ρ_m	Mixture density	(kg/m^3)
σ_t	Prandtl/Schmidt number	(-)
τ_p	Particle relaxation time	(sec)
$\vec{v}_m$	Mass-averaged velocity	(-)
$\vec{v}_{dr,k}$	Drift velocity for secondary phase *k* (velocity of an algebraic slip component relative to the mixture)	(-)
μ_m	Viscosity of the mixture	(N/m^2.s)

1-Water tank
2-Water pump
3-Valve
4-Water flow meter
5-Compressor
6-Air flow meter
7-Valve
8-Pressure sensor
9-Tringular cylinder
10-Tese section
11-Interphase
12-Personal computer

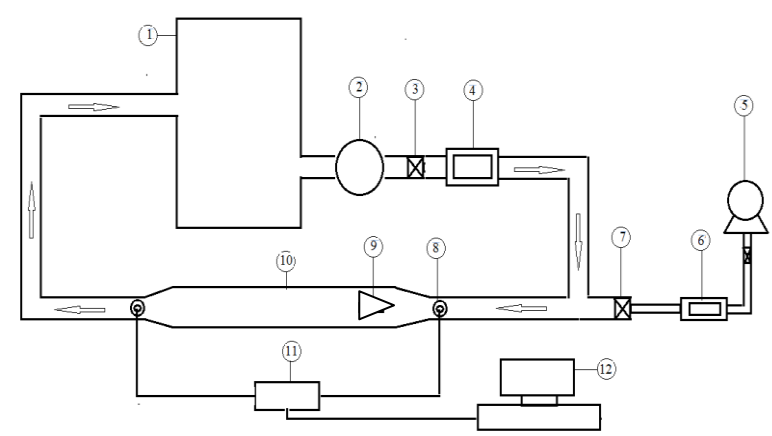

Figure 1 The experimental rig and measurements system (**Esam and Riyadh 2012)**.

(b) (c) (a)

Figure 2 (a) Water system, (b) Air flow meter, (c) Enlargement connecting part, flange, piping system and pressure transducer sensor (**Esam and Riyadh 2012)**.

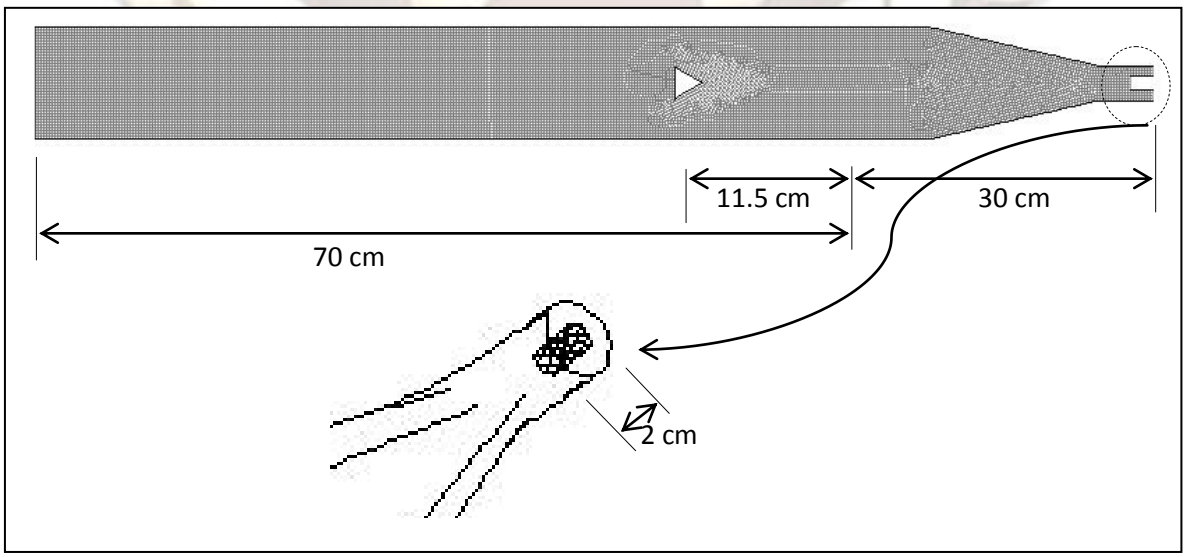

Figure 3. 2D model geometry structure mesh.

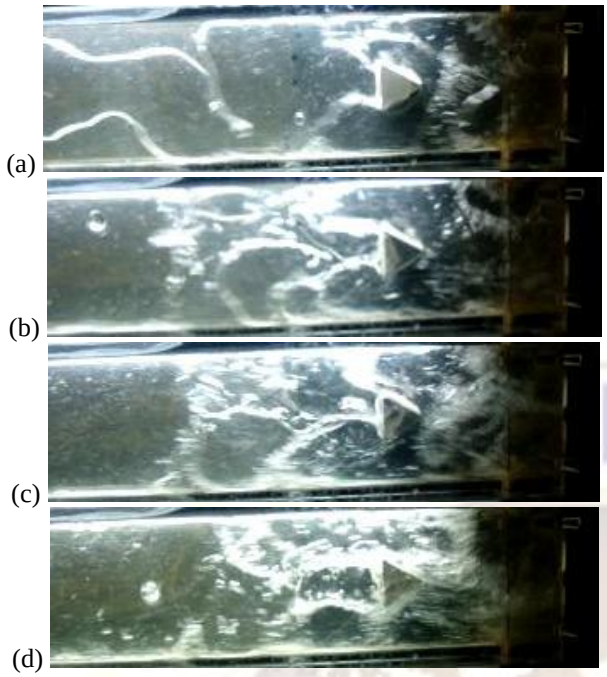

Figure 4 photographs for the two phase flow behavior for Q_a=10 l/min and Q_w=20, 25, 35 and 45 l/min respectively.

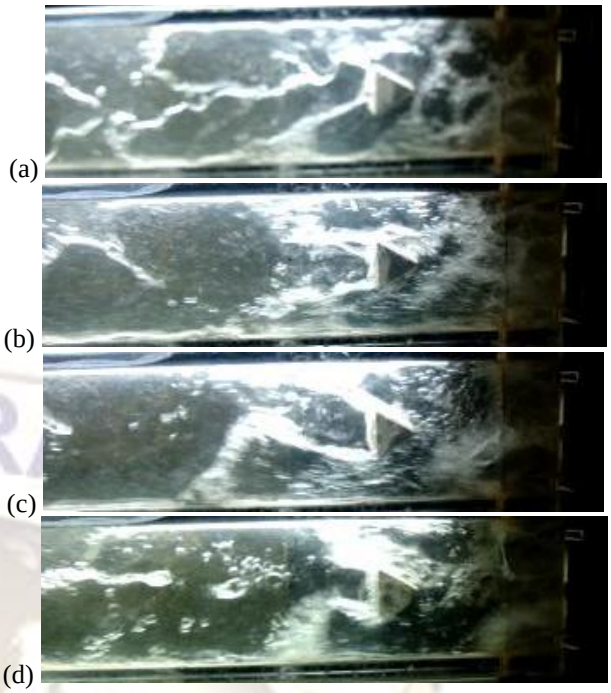

Figure 5 photographs for the two phase flow behavior for Q_a=20 l/min and Q_w=20, 25, 35 and 45 l/min respectively.

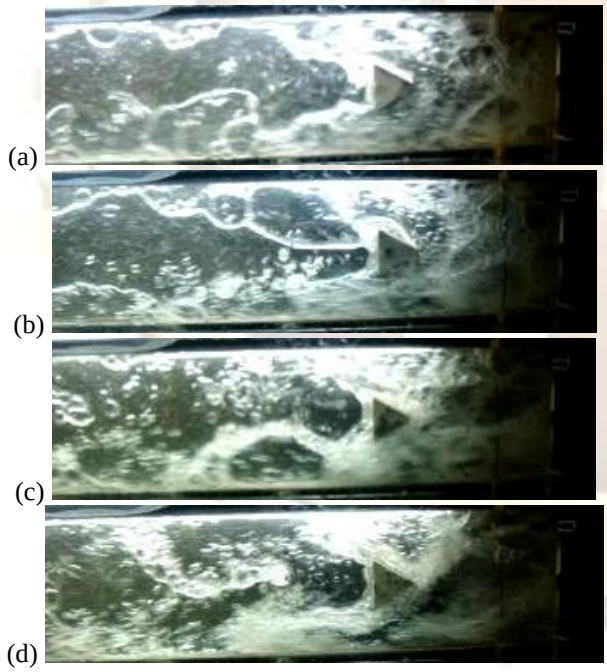

Figure 6 photographs for the two phase flow behavior for Q_a=30 l/min and Q_w=20, 25, 35 and 45 l/min respectively.

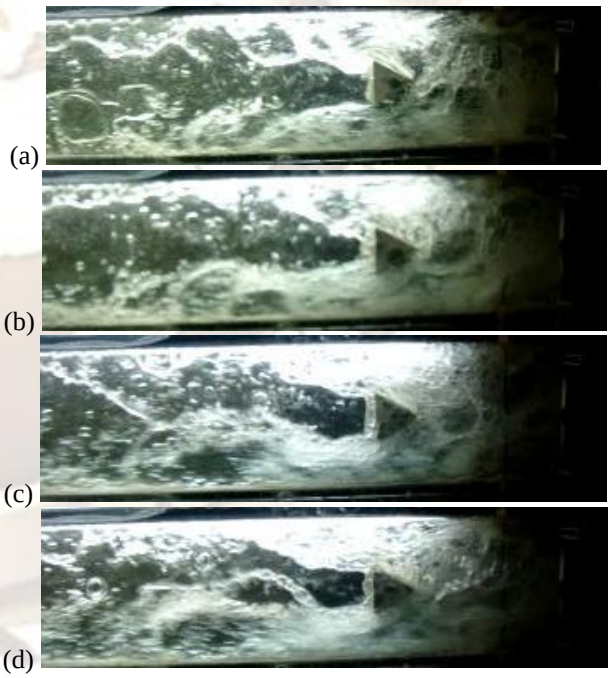

Figure 7 photographs for the two phase flow behavior for Q_a=40 l/min and Q_w=20, 25, 35 and 45 l/min respectively.

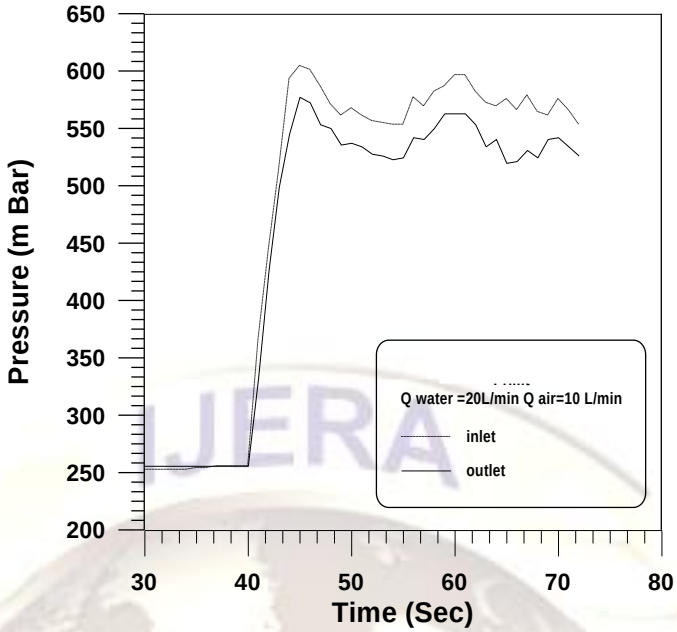

Figure 8 effect of time evolution of pressure for water discharge Q_w=20 l/min and air discharge Q_a=10 l/min.

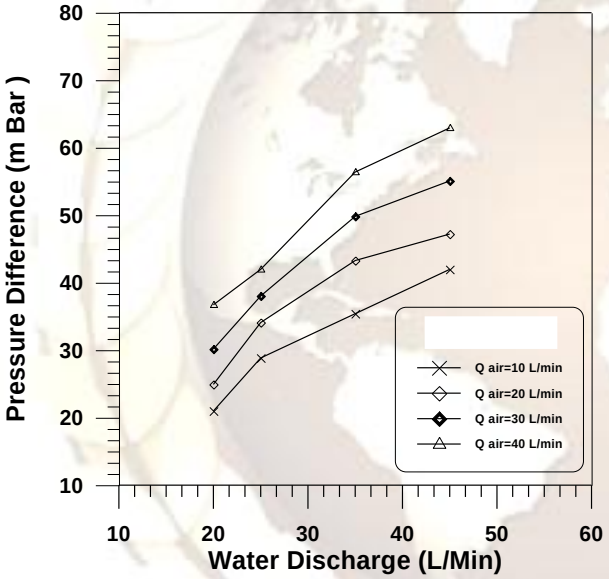

Figure 9 mean pressure difference with water discharge for different values of air discharge.

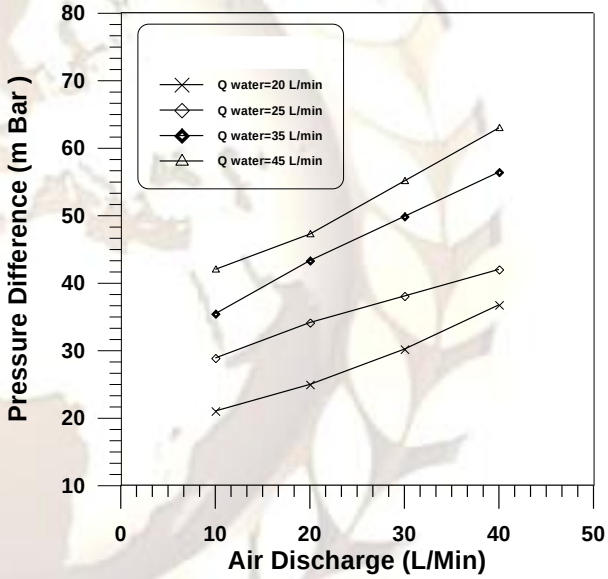

Figure 10 mean pressure difference with air discharge for different values of water discharge.

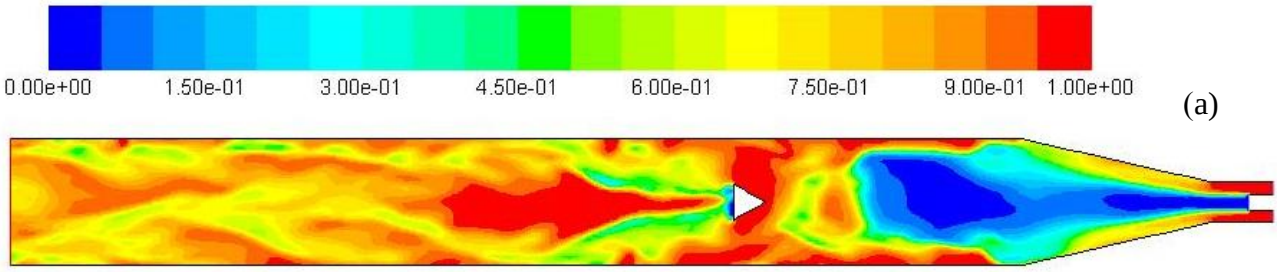

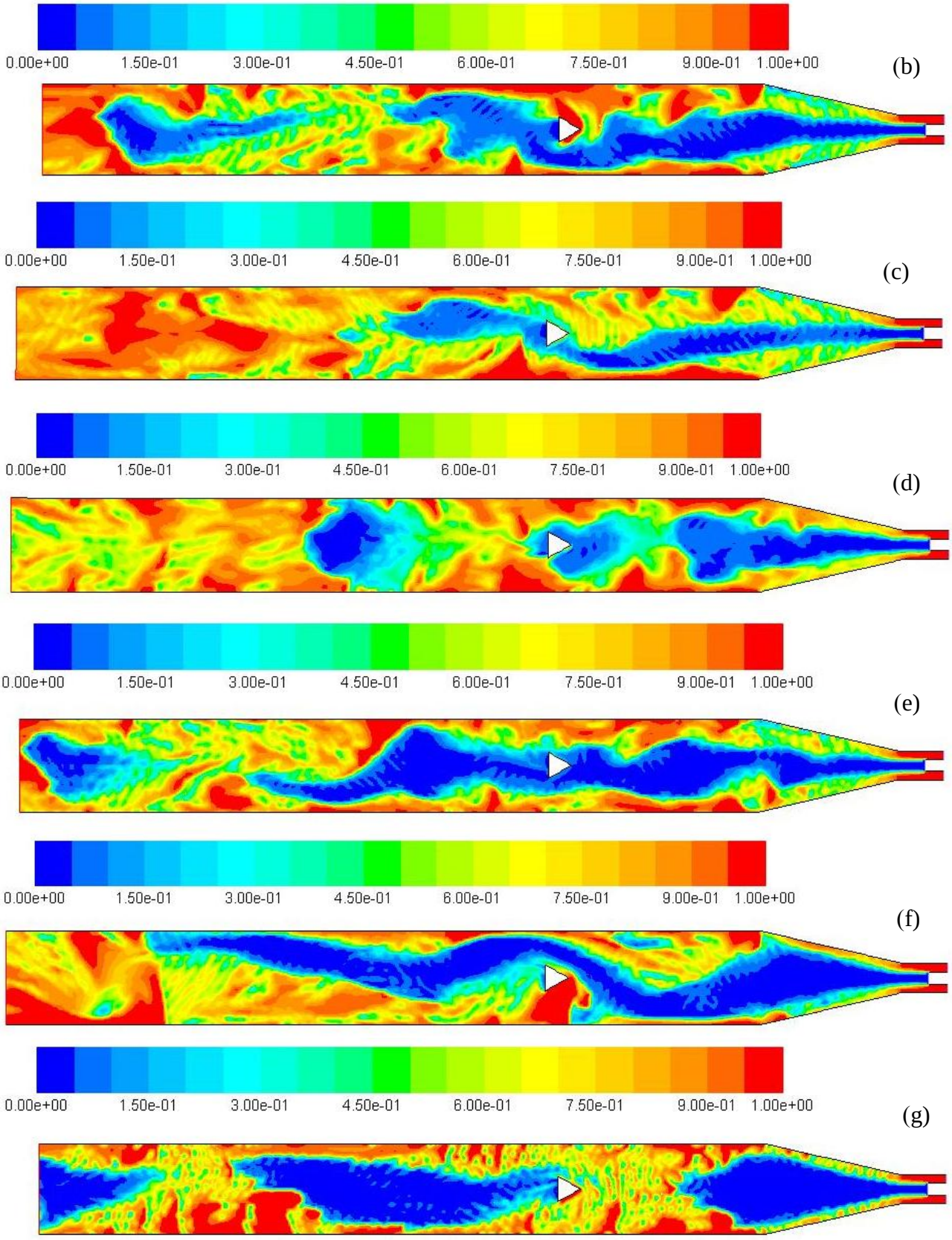
0.00e+00 1.50e-01 3.00e-01 4.50e-01 6.00e-01 7.50e-01 9.00e-01 1.00e+00
(b)
0.00e+00 1.50e-01 3.00e-01 4.50e-01 6.00e-01 7.50e-01 9.00e-01 1.00e+00
(c)
0.00e+00 1.50e-01 3.00e-01 4.50e-01 6.00e-01 7.50e-01 9.00e-01 1.00e+00
(d)
0.00e+00 1.50e-01 3.00e-01 4.50e-01 6.00e-01 7.50e-01 9.00e-01 1.00e+00
(e)
0.00e+00 1.50e-01 3.00e-01 4.50e-01 6.00e-01 7.50e-01 9.00e-01 1.00e+00
(f)
0.00e+00 1.50e-01 3.00e-01 4.50e-01 6.00e-01 7.50e-01 9.00e-01 1.00e+00
(g)

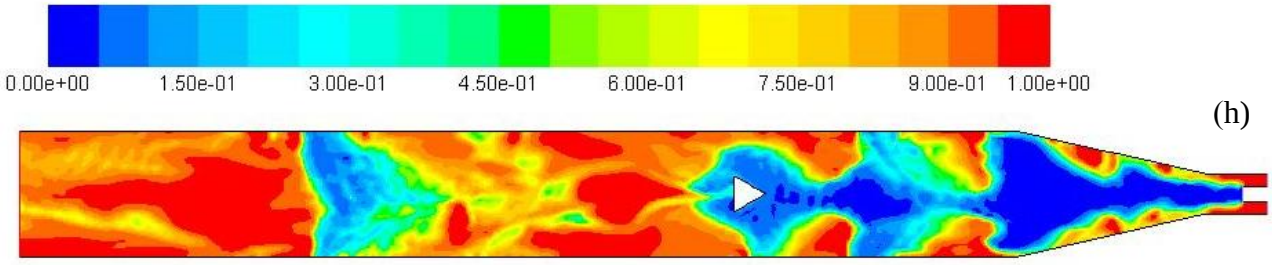

Figure 11 volume fraction (water) contours for cases (1, 2, 4, 5, 8, 11, 12 and 13) respectively.

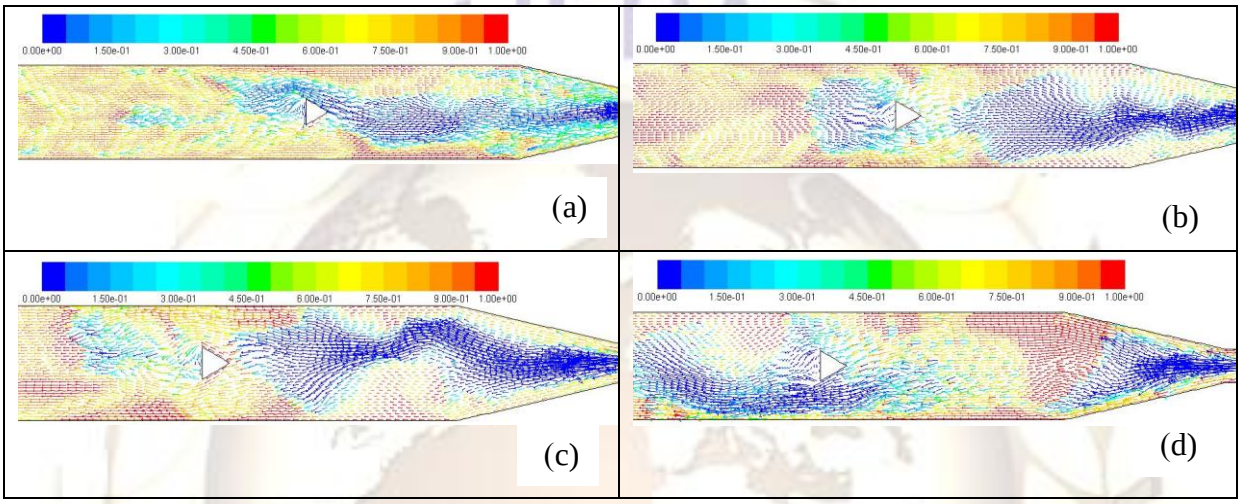

Figure 12 velocity vectors colored by volume fraction for cases (7, 10, 14, and 15) respectively.

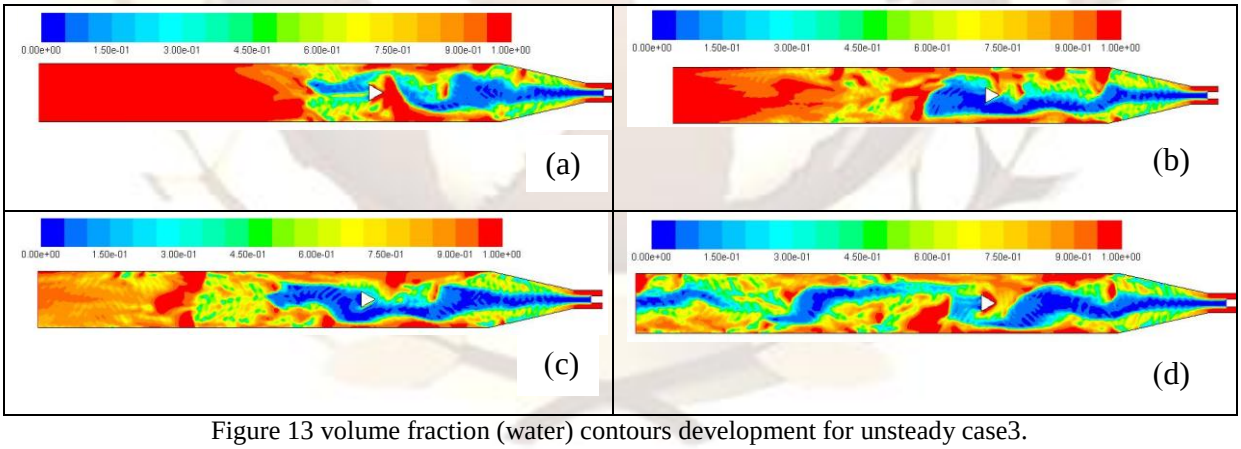

Figure 13 volume fraction (water) contours development for unsteady case3.